An Initial Intercomparison of Atmospheric and Oceanic Climatology for the ICE-5G and ICE-4G Models of LGM Paleotopography

F. JUSTINO

Department of Physics, University of Toronto, Toronto, Ontario, Canada

A. TIMMERMANN

IPRC, SOEST, University of Hawaii at Manoa, Honolulu, Hawaii

U. MERKEL

Leibniz Institut für Meereswissenschaften, IfM-GEOMAR, Kiel, Germany

W. R. PELTIER

Department of Physics, University of Toronto, Toronto, Ontario, Canada

(Manuscript received 14 March 2005, in final form 19 July 2005)

ABSTRACT

This paper investigates the impact of the new ICE-5G paleotopography dataset for Last Glacial Maximum (LGM) conditions on a coupled model simulation of the thermal and dynamical state of the glacial atmosphere and on both land surface and sea surface conditions. The study is based upon coupled climate simulations performed with the ocean–atmosphere–sea ice model of intermediate-complexity Climate de Bilt-coupled large-scale ice–ocean (ECBilt-Clio) model. Four simulations focusing on the Last Glacial Maximum [21 000 calendar years before present (BP)] have been analyzed: a first simulation (LGM-4G) that employed the original ICE-4G ice sheet topography and albedo, and a second simulation (LGM-5G) that employed the newly constructed ice sheet topography, denoted ICE-5G, and its respective albedo. Intercomparison of the results obtained in these experiments demonstrates that the LGM-5G simulation delivers significantly enhanced cooling over Canada compared to the LGM-4G simulation whereas positive temperature anomalies are simulated over southern North America and the northern Atlantic. Moreover, introduction of the ICE-5G topography is shown to lead to a deceleration of the subtropical westerlies and to the development of an intensified ridge over North America, which has a profound effect upon the hydrological cycle. Additionally, two flat ice sheet experiments were carried out to investigate the impact of the ice sheet albedo on global climate. By comparing these experiments with the full LGM simulations, it becomes evident that the climate anomalies between LGM-5G and LGM-4G are mainly driven by changes of the earth's topography.

1. Introduction

The impact of large-scale topography on both dynamical and thermodynamical aspects of planetary climate has been the subject of many investigations that have focused on both present and past climates regimes (e.g. Peltier and Solheim 2004; Vettoretti et al. 2000; Kitoh 2004; Kageyama and Valdes 2000; Kitoh 1997; Kasahara et al. 1973; Broccoli and Manabe 1987; Kutzbach and Guetter 1986; Manabe and Broccoli 1985; Manabe and Terpstra 1974). Kitoh (1997) and Seager et al. (2002) in particular demonstrated that present-day topographic features such as the Tibetan plateau and the Rocky Mountains play a key role in controlling the land and sea surface temperatures in high latitudes, primarily due to the role of these features in increasing tropospheric cloudiness, in inducing downstream atmospheric circulation changes, and through the direct effect of lapse rate. Previous coupled global climate model (CGCM) experiments (e.g. Kitoh 2004) demonstrated that systematic changes occur in the precipita-

Corresponding author address: Dr. F. Justino, Department of Physics, University of Toronto, 60 St. George St., Toronto, Ontario M5S 1A7, Canada.
E-mail: fjustino@atmosp.physics.utoronto.ca

© 2006 American Meteorological Society

tion and atmospheric circulation, as well as in sea surface temperature in response to increasing mountain uplift. The direct topographic influence on the climate has also been highlighted in modeling experiments focusing on the climate during the last glacial period (Justino et al. 2005; Peltier and Solheim 2004; Vettoretti et al. 2000; Felzer 2001; Kageyama and Valdes 2000; Cook and Held 1988; Rind 1987). These studies demonstrated that the glacial wintertime atmospheric circulation in the northern hemisphere (NH) during the Last Glacial Maximum (LGM) was more strongly influenced by the direct influence of glacial topographic forcing than by any other effect such as albedo, orbital forcing, and CO_2. For example, the topographic barrier provided by the presence of the Laurentide ice sheet over the northern part of the North American continent creates an upstream-blocking situation over the North Pacific, which significantly decelerates the westerlies (Justino et al. 2005; Timmermann et al. 2004). In addition, the ice sheet topography affects lee cyclogenesis over North America and generates stationary wave anomalies, which in turn play a key role in the baroclinic structure of the mean flow (Vettoretti et al. 2000; Kageyama and Valdes 2000).

Based on the topographically self-consistent version of the theory of postglacial relative sea level change and isostatic rebound, Peltier (1994) provided a paleotopography (ICE-4G) that, compared to today's topography, is characterized by the presence of vast continental ice sheets over North America, Scandinavia, and east Siberia. Recently, a refinement of this global ice sheet reconstruction (ICE-5G) has become available (Peltier 2004). This dataset differs significantly from the previous ICE-4G dataset at all NH locations that were glaciated at LGM. These locations include northwestern Europe/Eurasia (Peltier 2004; Peltier et al. 2002), the British Isles (Peltier et al. 2002), Greenland (Tarasov and Peltier 2002), and the North American continent (Peltier 2004). For instance, the western flank of the Laurentide ice sheet in the ICE-5G reconstruction is approximately 1500 m higher whereas the Greenland ice sheet is approximately 500 m lower in the ICE-5G model as compared to the ICE-4G model. Furthermore, the topographic feature related to the ice sheet on the East Siberian Shelf that was included in the ICE-4G dataset has been entirely eliminated from the ICE-5G dataset (see Fig. 1a). The new ICE-5G dataset is also characterized by a distinct difference in the ice sheet mask as compared to its predecessor, ICE-4G. The highly significant changes in surface albedo (Fig. 1b) are located over Eurasia due to the elimination of the extensive ice cover in this region that was contained in the ICE-4G model. These changes lead, in ICE-5G, to a reduction of surface albedo over this region by up to 40%.

In the present paper, our goal is to provide an initial investigation of the impact of the new paleotopography (ICE-5G), and associated albedo changes, on the atmospheric circulation and on land and sea surface conditions during the Last Glacial Maximum. The comparison will be based on an LGM climate experiment using the ICE-5G topography (LGM-5G hereafter) and a reference LGM experiment performed with the ICE-4G topography (LGM-4G hereafter). To investigate the impact of the ice sheet mask, two flat ice sheet experiments will be analyzed. The paper is organized as follows: Section 2 describes the coupled atmosphere–ocean–sea ice model and the design of the two experiments. In section 3, the main results are presented. Section 4 summarizes the main findings and provides a discussion of the limitations of the modeling approach that we have employed for the purpose of this initial assessment of the implication of the revised ICE-5G LGM paleotopography.

2. The coupled climate model and the design of the numerical experiments

The atmospheric component Climate de Bilt (ECBilt) (Opsteegh et al. 1998) of our coupled model is a three-layer model with a quasigeostrophic adiabatic core, ageostrophic parameterizations (Marshall and Molteni 1993), a set of physical parameterizations for the hydrological cycle (Held and Suarez 1978; Opsteegh et al. 1998), and a simplified radiation code. It is a spectral model that is run at T21 triangular truncation, which corresponds to an approximate resolution of 5.6° in both latitude and longitude. At the top of the atmosphere ($p = 0$), the rigid lid $\omega = 0$ is applied. At the lower boundary, ω is a function of vorticity and the rotational velocity, of the surface drag coefficient, and of density and orographic height {i.e., $\omega_s = -\rho_s g[(C_D/f_o)\zeta_s - V_{\zeta s} \cdot \nabla h]$}. Here $\omega = (\partial p/\partial t)$ is the vertical velocity in isobaric coordinates; ζ_s and $V_{\zeta s}$ are the vorticity and the rotational velocity at the top of the boundary layer, respectively, for which the values at 800 hPa are chosen; C_D is the surface drag coefficient; ρ_s is the density at the surface; and h is the orography height. The coupled large-scale ice–ocean model Clio (Goosse et al. 1999; Goosse and Fichefet 1999; Goosse et al. 2003) is based on the primitive equations and employs a free surface for the ocean component and thermodynamic/dynamic assumptions for the sea ice component. A parameterization for vertical mixing (Goosse et al. 1999) is employed that constitutes a simplification of the Mellor and Yamada 2.5-level turbulence closure scheme

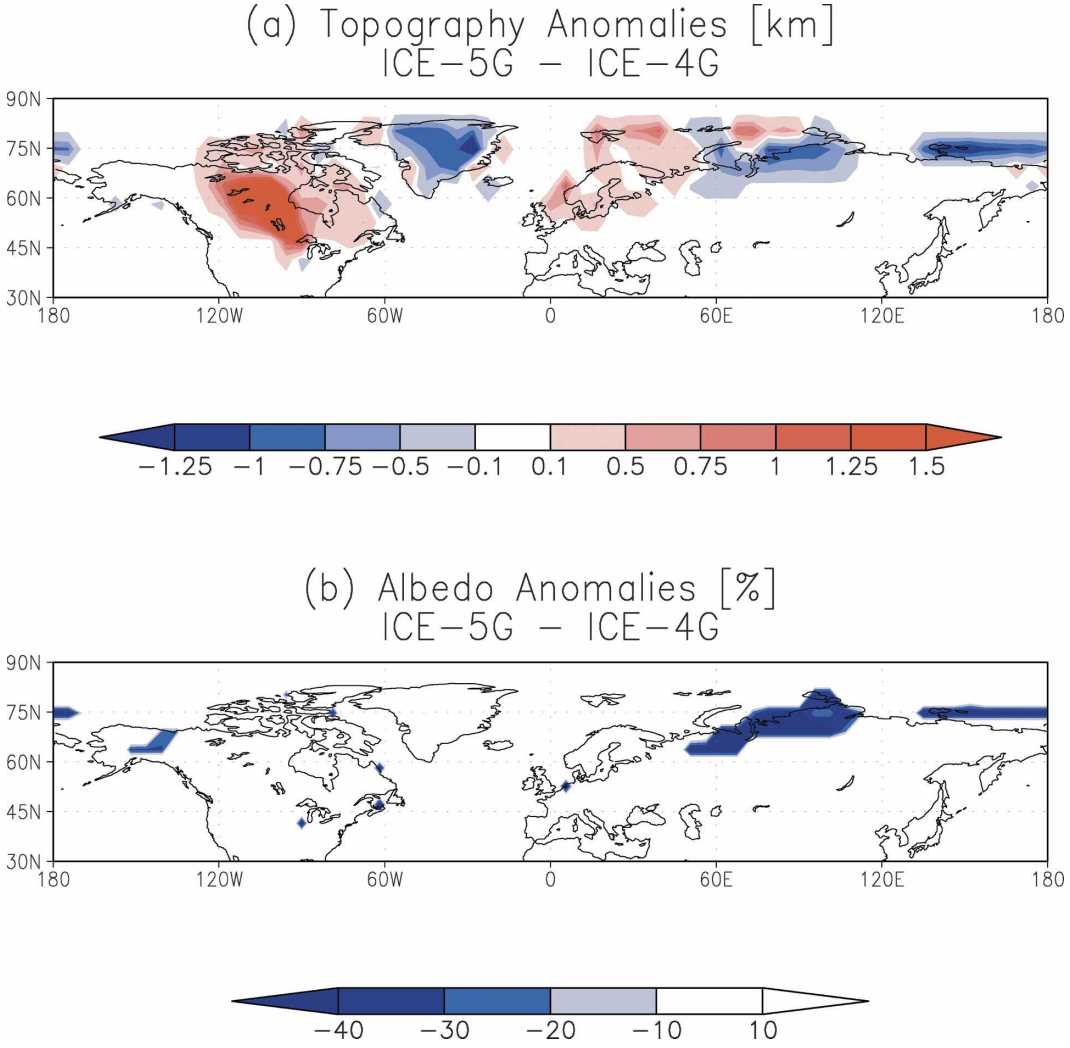

FIG. 1. (a) Paleotopography anomalies between ICE-5G and ICE-4G in the NH (km). (b) Same as in (a), but for albedo. The changes in topography and albedo in the SH are very small and they are not shown here.

(Mellor and Yamada 1982). Furthermore, the ocean model Clio includes mixing along isopycnals such as to capture the impact of mesoscale eddies on the transport (Gent and McWilliams 1990) as well as the flow of dense water down topographic features (Campin and Goosse 1999). The horizontal resolution of the Clio model is 3°, and there are 20 unevenly spaced vertical levels in the ocean. The individual models are coupled through exchanges of momentum, freshwater, and heat, and the simulations are performed using weak freshwater flux corrections so as to inhibit climate drift. The results that we have obtained using this Earth System Model of Intermediate complexity (EMIC) will be tested against the predictions of more sophisticated models of the coupled climate system such as the National Center for Atmospheric Research (NCAR) Climate System Model (CSM) in a future publication based on work that is currently in progress.

In order to investigate the atmospheric response to the ICE-5G topography, five experiments were conducted. The first experiment is a simulation of preindustrial climate. This employed an atmospheric CO_2 concentration of 280 ppm and present-day albedo, vegetation, orbital forcing, and topographic boundary conditions (for details see Timmermann et al. 2004). In the LGM-4G and LGM-5G experiments, we prescribe a reduced atmospheric CO_2 concentration (200 ppm), appropriate LGM orbital forcing (Berger 1978), and an appropriate LGM vegetation mask (e.g. Crowley 1995) for which the deforested soils and plant cover are replaced by their respective glacial albedos. Ice sheet albedo is set to 0.8.

The incorporation of the influence of the ice sheet albedo increases the area mean surface albedo in North America and Eurasia by more than 60% compared to preindustrial initial conditions. The LGM-4G and LGM-5G simulations therefore differ only in the paleotopographies and albedos employed at the lower boundary of the atmosphere. The respective ice sheet topography is included as an anomaly between the ICE-4G or ICE-5G reconstructions and present-day topography. This anomaly field is added to the default topography pattern of the atmospheric component of ECBilt-Clio (see Fig. 1 for the difference between the topography and albedo files). To differentiate climate anomalies associated with the mechanical effect of ice sheet paleotopographies from the effect of diabatic heating (albedo), we performed a pair of additional flat ice sheet experiments. These experiments differ by their ice sheet albedos and by the fact that all topography is set to zero over all continents (FLAT-5G and FLAT-4G hereafter). The associated changes of river runoff from the continents have not been included for the purpose of these analyses.

Both the LGM-4G and LGM-5G simulations were integrated for 1000 yr starting from the same initial conditions. The FLAT-5G and FLAT-4G simulations were integrated for 300 yr starting from equilibrated LGM-4G and LGM-5G simulations. Our analyses focus on the last 100 yr of the simulations after the model had reached the new state of "statistical equilibrium," which is characterized by vanishing secular drift of surface temperature. Since the LGM-4G simulation has been discussed in detail in previous publications (Justino et al. 2005; Timmermann et al. 2004), no purpose will be served by discussing this in detail herein, although a very brief review of these results will prove useful. In comparison with the preindustrial climate simulation, the LGM-4G results exhibit an overall surface cooling except for the North Pacific, in which a warming occurs that may be attributed to a topographically induced modification of the large-scale atmospheric circulation (see Timmermann et al. 2004). The SST anomalies in the North Atlantic delivered by this simulation bear many similarities with the more recent SST reconstruction of Glacial Atlantic Ocean Mapping (GLAMAP; Schäfer-Neth and Paul 2003). Furthermore, the Laurentide ice sheet is shown to induce an upstream blocking situation whereas the downstream expected low pressure region interacts with the upstream high generated by the European ice sheet, consistent with the theoretically expected effect of topography on the atmospheric circulation (e.g. Manabe and Terpstra 1974). In addition, stationary wave patterns in summer simulated by LGM-4G appear to be very sensitive to diabatic forcing due to albedo changes in the NH in agreement with previous studies (Vettoretti et al. 2000; Cook and Held 1988; Rind 1987; Broccoli and Manabe 1987). The simulated glacial rainfall in the LGM-4G simulation (reference LGM simulation) is also consistent with lake-level reconstructions (Kohfeld and Harrison 2000) and with the existence of a permanent La Niña state, as discussed previously by Timmermann et al. (2004). The comparison between the simulated temperature of the coldest month and the paleoreconstructions (Farrera et al. 1999) also shows good agreement in the equatorial zone. Over the subtropics, however, the LGM-4G simulation underestimates the cooling. This may be compared with the recently published LGM results by Peltier and Solheim (2004), who employed version 1.4 of the NCAR CSM model and obtained results for tropical cooling that are in close accord with results based upon proxy SST reconstructions. The latter simulation of LGM climate also predicted significantly enhanced power for the LGM ENSO. One goal of the ongoing reanalysis of LGM climate using the NCAR CSM is to determine whether or not this result can be considered robust.

3. Results and discussion

a. Changes in the circulation of the atmosphere

In what follows, the joint effect of changes in topography and albedo on LGM climate are discussed. Climate anomalies induced solely by albedo changes are discussed afterward. Due primarily to the lapse rate effect, the surface temperature anomalies (Fig. 2a) over land in general follow the changes in glacial topography, in particular the enhanced topographic heights in the northern part of the North American continent and in Scandinavia. Lower temperatures, by up to 5°C, are found over northern North America and by up to 2°C over Eurasia in the LGM-5G simulation as compared to the LGM-4G simulation (Fig. 2a). It is important to note that with respect to preindustrial conditions this represents a net surface cooling over the ice sheets of up to 25°C. This cooling results from the combined effects of several contributions: namely the lapse rate effect, the reduction in the mass of the atmosphere above the elevated ice sheet, and the albedo increase associated with a larger seasonal area covered by snow. Over North America (Eurasia), the specific humidity (amount of water vapor in the air) is reduced by about 25% (35%) in the LGM-5G simulation compared to the LGM-4G counterpart, a highly significant effect. Because of this reduction of specific humidity, the longwave radiative loss to space is increased. Furthermore, due to the enhanced wintertime rate of snow accumu-

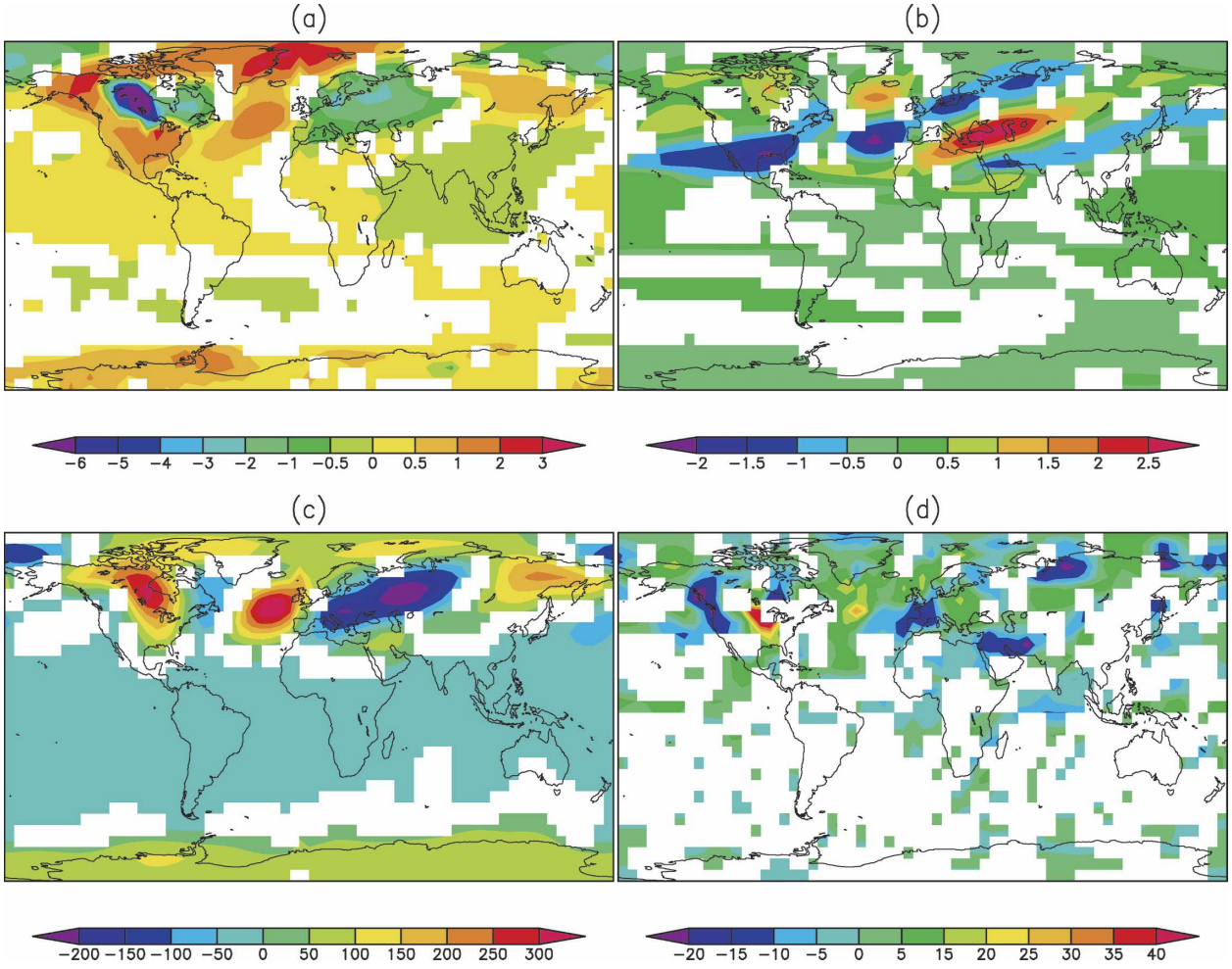

FIG. 2. Annual mean anomalies between LGM-5G and LGM-4G simulations. (a) Surface temperature (°C), (b) wind at 200 hPa (m s^{-1}), (c) geopotential height (m^2 s^{-2}), and (d) is precipitation (cm yr^{-1}). Shaded areas are statistically significant at the 95% level.

lation and an associated higher surface albedo (in particular over Scandinavia and central Asia), the LGM-5G simulation results in a reduction in absorbed solar radiation by up to 10% over the Eastern Hemisphere (not shown). In the LGM-5G simulation, higher surface temperatures with respect to the LGM-4G simulation are however found over southern North America, the Labrador Sea, and the North Atlantic/Greenland and over east Asia and the SH extratropics (Fig. 2a). The NH warming is apparently caused by the subsidence of air to the south and east of the topographic anomaly. A similar feature has been found by Rind (1987), in particular during the NH summer. The increased northward flow due to high pressure anomalies over North America (see Fig. 2c) may also contribute to higher temperature anomalies due to warm air advection. In addition, changes of oceanic surface conditions and the thermohaline circulation play a key role in enhancing the warming over the North Atlantic as discussed in the next section. Over eastern Greenland, however, the lapse rate effect due to the lower ice sheet elevation leads to higher surface temperatures in the LGM-5G simulation as compared to LGM-4G. Over most parts of the oceans, the surface temperature anomalies are characterized by warmer conditions in the LGM-5G simulation except for the northern part of the Indian Ocean (Fig. 2a). The global averaged annual surface temperatures in the two simulations (LGM-5G and LGM-4G) differ only by 0.1°C.

Due to the simulated changes in temperature discussed above, significant changes of the atmospheric circulation may also be expected. Since the topographic changes between the two simulations are mainly located in the NH, one would expect that the largest wind anomalies would also develop in the NH. Indeed, at 500 hPa the most prominent differences between the

LGM-4G and LGM-5G simulations are cyclonic and anticyclonic cells over the NH (Figs. 2b,c). Over central Europe in particular, the cyclonic wind anomalies contribute significantly to surface cooling (see Fig. 2a) due to cold air advection from the polar region. In the Western Hemisphere, on the other hand, anticyclonic wind anomalies appear over the Laurentide ice sheet itself and over the North Atlantic Ocean (Figs. 2b,c). Zonal wind changes at 200 hPa (Fig. 2b) indicate that the presence of the ICE-5G topography in place of the ICE-4G topography does result in a severe modification of the position of the jet stream (Fig. 2b). The maxima of jet stream intensity over the east coasts of North America and Asia have almost the same magnitude in the LGM-4G and LGM-5G simulations. A significant difference in the zonal velocities is shown to develop in the subtropical region of the Western Hemisphere (Fig. 2b). Furthermore, areas of stronger winds are predicted to develop in the midlatitudes over middle-eastern/central Asia as well as in the region from the northeastern Pacific to the North Atlantic. Upper-level wind changes over the SH, in comparison, are relatively small. It will be of great interest to determine the robustness of this result to the introduction of a much more accurate description of the atmospheric general circulation as contained, for example, in the NCAR CSM.

As a result of strong surface cooling related to the increased elevation of the Laurentide ice sheet in the ICE-5G dataset compared to that in ICE-4G, the predicted 500-hPa geopotential height anomalies are characterized by the presence of an anticyclonic circulation anomaly over North America (Fig. 2c). In addition, a wave-like structure in the NH is clearly evident in Fig. 2c. This structure induces a warming (cooling) of western (eastern) North America in the LGM-5G simulation due to the thermal advection from the south (north) (Fig. 2a). A high pressure feature also develops as the downstream response to the modification of the Fennoscandian ice sheet in the ICE-5G model compared to its form in ICE-4G (Fig. 2c). This topographic response has been described in several studies (Justino et al. 2005; Timmermann et al. 2004; Felzer 2001; Cook and Held 1988; Rind 1987). Furthermore, in the LGM-5G experiment, an increase in 500-hPa geopotential height is simulated over northeastern Asia. Regions of low pressure anomalies and associated cyclonic winds are found over Eurasia as a result of the topographic changes in the Fennoscandian ice sheet in the ICE-5G dataset. This can be in part understood on the basis of considerations based upon the conservation of potential vorticity. Westerly flows incident upon topographic barriers typically generate downstream cyclonic circulation and anticyclonic circulation upstream of the topographic barrier. It must be noted, however, that the advection of polar air also plays a key role in generating the trough over Eurasia because it leads to a reduction of the thickness of the column, and hence the height of the 500-hPa surface decreases. This effect seems to be dominant in generating the high pressure anomalies over the Laurentide ice sheet due to warm air advection. A detailed description of the influence of thermal advection on geopotential height was provided by Holton (1993). Before discussing changes in precipitation, it is interesting to investigate the impact of ICE-5G topography on the baroclinic structure of the atmosphere. This may be approximately quantified in terms of the Eady growth rate (Lindzen and Farrell 1980). This is a measure of the baroclinicity of the atmosphere and can be employed to quantify the potential for instability and cyclone growth. The Eady growth rate estimates baroclinic instability through the vertical wind shear and the static stability in the atmosphere. It is defined as $\sigma_{\mathrm{BI}} = 0.31(f/N)|\partial v/\partial z|$, where f is the Coriolis parameter, N is the Brunt-Väisälä frequency, z is the upward vertical coordinate, and v is the horizontal wind. The Eady growth rate anomalies between the LGM-5G and the LGM-4G simulation (Fig. 4a) exhibit an increase in baroclinicity of about 10%, in particular over North America, Siberia, and central Asia. This increase in the degree of baroclinic instability of the zonal flow is primarily a consequence of the steeper meridional temperature gradient that is characteristic of the LGM-5G simulation. This strengthening in the baroclinic activity plays an important role in modifying the snow accumulation rates and thus may play a key role on the ice sheet mass balance, especially over the Laurentide ice sheet. These results are corroborated by analyzing the transient eddy kinetic energy changes (not shown).

Temperature changes as well as changes of the eddy activity of the atmosphere are related to changes in the hydrological cycle in the extratropics. Precipitation changes over the Tropics when using the ICE-5G instead of the ICE-4G topography are negligible. The largest positive precipitation anomalies are found over southern North America and the North Atlantic (Fig. 2d). The higher LGM topography in the ICE-5G dataset over North America induces an uplift of the air leading to condensation and precipitation. In addition, the strong meridional thermal contrast over North America (Fig. 2a) is associated with enhanced baroclinicity (Fig. 4a) and thus with enhanced midlatitude cyclogenesis. These frontal systems are typically accompanied by precipitation and snowfall, even in the ECBilt-Clio model, which employs simplified physical

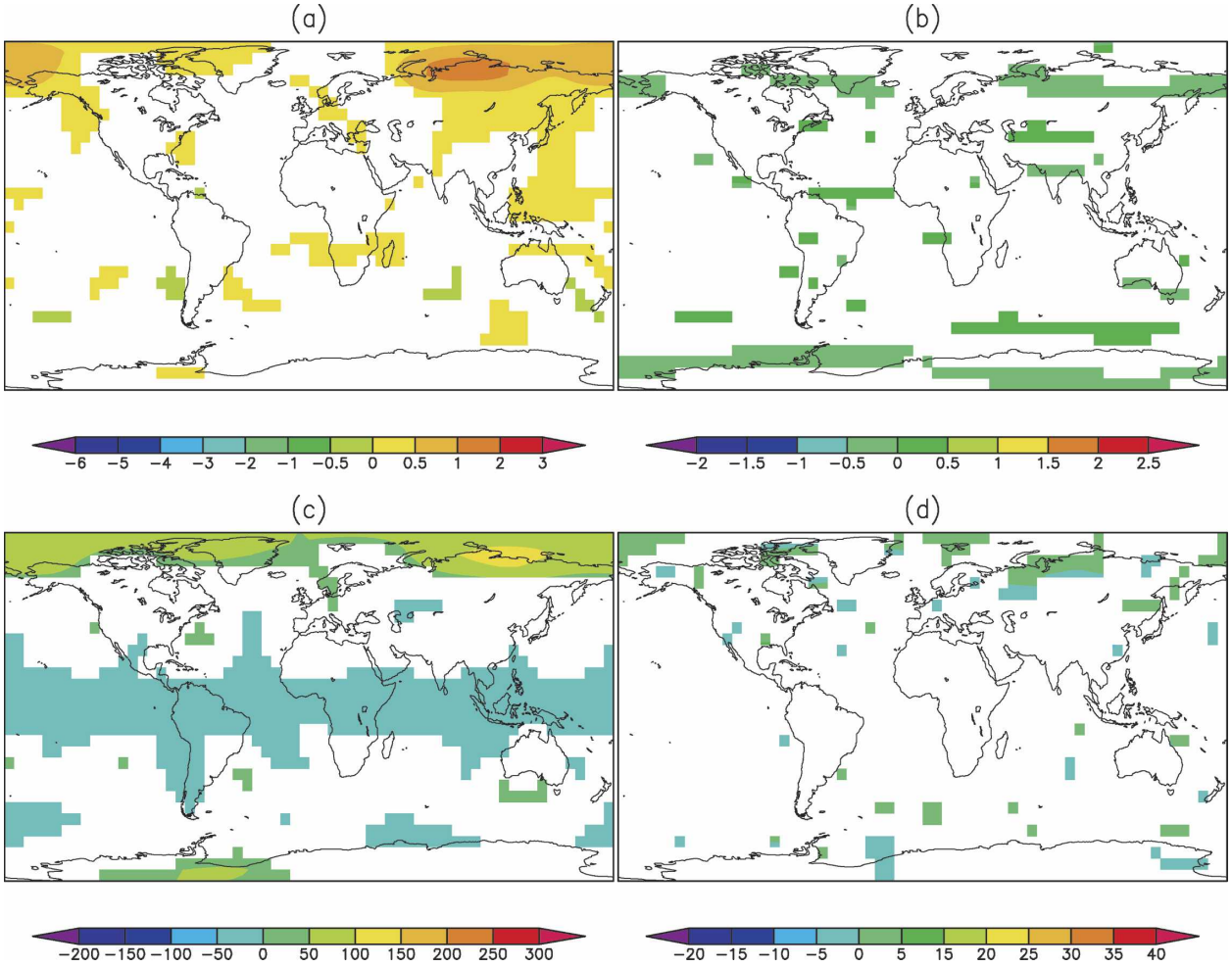

FIG. 3. Same as in Fig. 2, but for FLAT-5G and FLAT-4G simulations.

parameterizations. Over the western North Atlantic, wetter conditions seem to be related to the low pressure system anomalies that form over the Labrador Sea (see Fig. 2c). Furthermore, it can be argued that changes in baroclinicity may have a large impact on the North Atlantic storm track and consequently upon the associated precipitation.

b. The flat ice sheet simulations

To separate the climate response due to changes in topographic height from those due to the ice sheet albedo feedback, the flat ice sheet simulations have been analyzed for comparison purposes. As is evident from Fig. 3, changes in ice sheet albedo between the LGM-5G and LGM-4G simulations in general play a secondary role in generating major climate anomalies. Nevertheless, some differences are noticeable between the two flat ice sheet simulations (FLAT-5G and FLAT-4G) from Siberia to Alaska. For instance, the absence of the ice sheet albedo over Eurasia (Fig. 1b) decreases the surface albedo leading to warmer surface conditions in the FLAT-5G simulation compared to the FLAT-4G simulation (Fig. 3a). Globally averaged the FLAT-4G simulation is 0.3°C colder than the FLAT-5G simulation. Turning to changes of the upper-level jet stream (200 hPa) (Fig. 3b), it is clear that the modification of ice sheet albedo between the ICE-5G and ICE-4G dataset does not produce significant changes of the predicted jet stream. However, a slight intensification of the SH westerlies is predicted to occur over the Indian Ocean in the FLAT-5G simulation. On the other hand, the presence of lower surface albedo due to the elimination of the ice sheet on the East Siberian Shelf in FLAT-5G leads to positive geopotential height anomalies in the NH polar region (Fig. 3c). By comparing the surface temperature and geopotential height anomalies, it is clear that surface changes substantially affect the climate in the middle troposphere. Given this, one

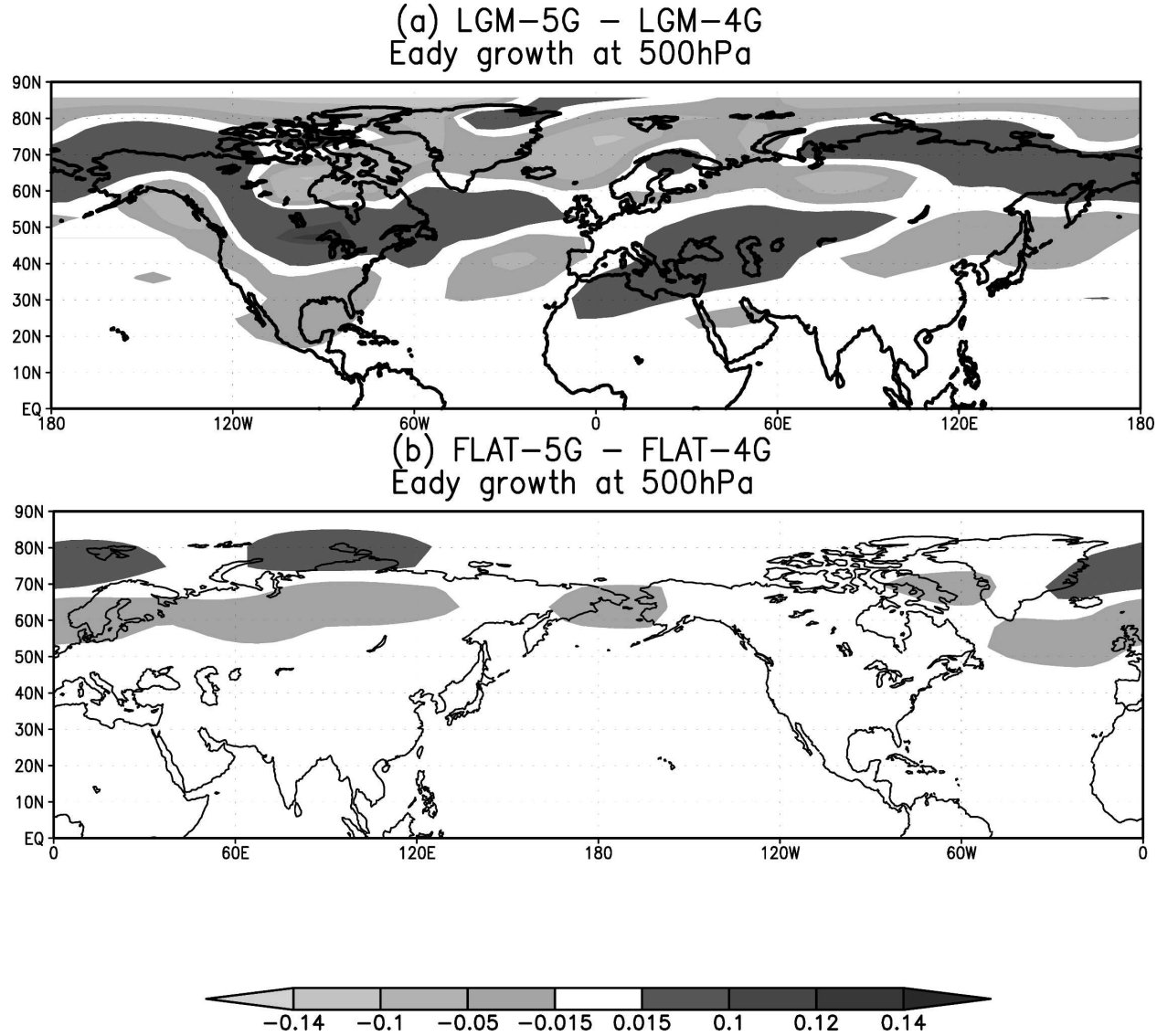

FIG. 4. Annual mean Eady growth rate anomalies (day^{-1}). (a) LGM-5G − LGM-4G and (b) FLAT-5G − FLAT-4G. Positive values correspond to enhanced baroclinic instability.

can argue that changes of sea ice albedo feedback, perhaps associated with an expected increase of atmospheric greenhouse gases concentration, may trigger an anomalous middle-troposphere circulation over the NH polar region that can feed back on the initial surface anomalies. Changes in precipitation between FLAT-5G and FLAT-4G simulations are found downstream of Scandinavia (Fig. 3d) close to the region where the albedo was modified. Moreover, this matches with positive eady growth rate anomalies, that is, enhanced baroclinic activity, as shown in Fig. 4b. Elsewhere the anomalies are in general not statistically significant at the 95% level. It is reasonable to assume that the climate impact of changes in ice sheet albedo is not prominent because the surface albedo changes between the two ice sheet models are very small (Fig. 1b).

c. *Changes in the circulation of the oceans*

Topographically induced changes of the atmospheric circulation may have a large impact on upper-ocean dynamics and thermodynamics. We focus on changes in the NH because oceanic surface condition in the SH hardly change in the LGM-5G simulation compared with the LGM-4G simulation. SST differences between the LGM-5G and LGM-4G experiments show a warming by up to 2°C in the North Atlantic and by up to 0.5°C in the northeastern Pacific (Fig. 5a). The strong northward wind anomaly over the North Atlantic at

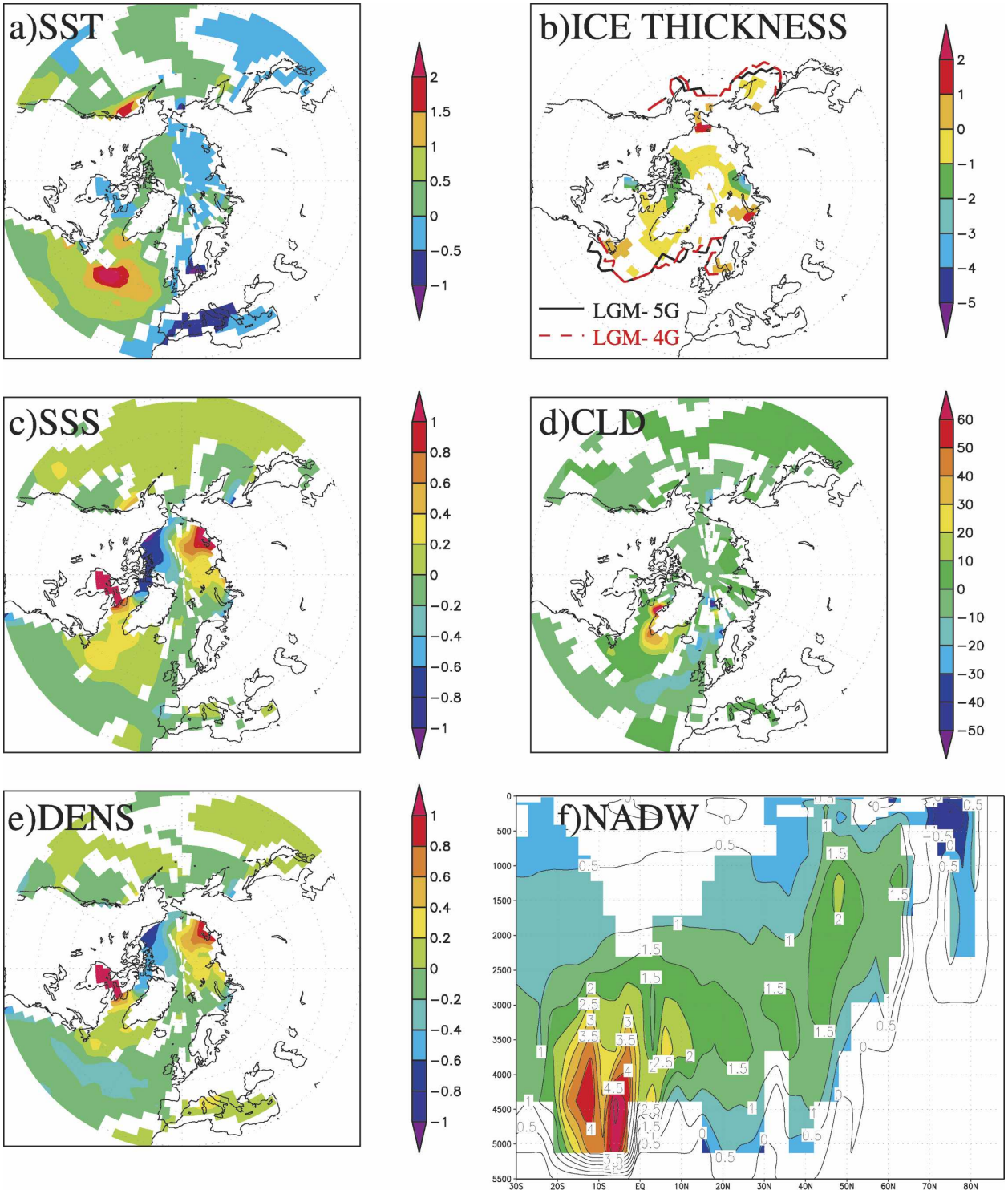

FIG. 5. Annual mean anomalies between LGM-5G and LGM-4G simulations for (a) surface surface temperature (°C), (b) sea ice thickness (m), (c) surface surface salinity (psu), (d) convective layer depth (m), (e) surface density (kgm^{-3}), and (f) the Atlantic overturning circulation [Sv (1 Sv $\equiv 10^6$ m^3 s^{-1})]. The red and black lines in (b) depict the sea ice extent in the LGM-4G and LGM-5G simulations. Shaded areas are statistically significant at the 95% level.

800 hPa (not shown) intensifies the warm air advection from the subtropics, thus reducing the oceanic heat loss at higher latitudes. The wind anomalies also intensify the oceanic subtropical gyre in the North Atlantic as diagnosed by the Sverdrup relation (not shown). The stronger subtropical gyre enhances the transport of warm and salty waters from the tropical region to the extratropics, thereby favoring warmer midlatitude SSTs in LGM-5G compared to the LGM-4G simulation. In addition, the LGM-5G simulation exhibits reduced cold air advection from the Laurentide ice sheet, which in turn reduces the heat exchange between the ocean and the atmosphere. This effect is expected to be more robust in wintertime when the glacial NH atmospheric circulation is more active (Broccoli and Manabe 1987; Rind 1987). As a result of the warming over the Labrador Sea/North Atlantic, this region experiences a reduction of sea ice thickness in LGM-5G compared to the LGM-4G simulation (Fig. 5b). Moreover, thinner sea ice is predicted to occur from Siberia to the Canadian high Arctic archipelago. This is likely a result of warmer surface temperatures in the central Arctic Ocean/Greenland in the LGM-5G simulation compared to the LGM-4G simulation (see Fig. 2a). Increased sea ice thicknesses are simulated in the Kara and Barents Seas (Fig. 5b). No substantial changes in terms of sea ice extent are found between the LGM-5G and LGM-4G simulations.

Sea surface salinity (SSS) anomalies due to the presence of ICE-5G topography are striking compared to the reference simulation LGM-4G. Areas of enhanced SSS can be found in the North Atlantic and Siberian Seas (Fig. 5c). The changes in the North Atlantic are in agreement with an increased evaporation/precipitation budget (E/P flux) in the LGM-5G simulation compared to the LGM-4G simulation (not shown) and lead to an increased wind-driven poleward salinity transport. It is important to note, moreover, that the strengthening of the North Atlantic subtropical gyre in the LGM-5G simulation (not shown) induces advection of subtropical salty waters to high latitudes. The SSS changes in Siberia seem to be associated with subsurface process because SST and sea ice anomalies do not favor an increase in SSS as predicted by the LGM-5G simulation. These SSS anomalies are clearly reflected on the convective layer depth and oceanic density changes in the Siberia and Labrador Seas (Figs. 5d,e).

These changes of oceanic surface conditions have an important impact on North Atlantic Deep Water formation (NADW) as discussed below. The strength of the NADW formation rate during the LGM is a controversial issue. For example, it is as yet unresolved as to whether the LGM climate exhibited stronger or weaker NADW compared to today's NADW. Paleoceanographic data (Veum et al. 1992) and other LGM model simulations (Hewitt et al. 2001; Kitoh et al. 2001) support the possibility of a stronger NADW. On the other hand, in the analysis of this characteristic of LGM climate discussed in Peltier and Solheim (2004) using the NCAR CSM 1.4 model, it was found that the Atlantic maximum overturning circulation (MOC) was reduced in intensity by approximately 40% compared to the modern control model, a result that is in close accord with the recent inference of McManus et al. (2004) based upon their use of the $^{231}Pa/^{230}Th$ tracer of the strength of the western boundary undercurrent. Compared to the simulated present-day NADW formation rate, our LGM-4G simulation predicts an enhancement of the NADW formation rate. Glacial cold air advection from the Laurentide ice sheet leads to thermal density flux anomalies, which in turn generates substantial changes in the surface density in the main sites of deep water formation (Justino 2004). Furthermore, deep convection occurs farther south in areas that are typically more saline than those associated with present-day deep convection.

Based on predicted SST anomalies (Fig. 5a) between LGM-4G and LGM-5G simulations, one should expect a weakening of the NADW formation rate in the later experiment. Nevertheless, this negative thermal effect is compensated by increased surface salinity (Fig. 5c) that leads to increased density in the LGM-5G simulation (Fig. 5e), which in turn leads to an enhanced NADW formation rate. As proposed by Schmitt et al. (1989) and Speer and Tziperman (1992), surface density anomalies (Fig. 5e) can generate thermohaline circulation changes. These anomalies result mainly from a combination of variations of the thermal and the haline fluxes. Despite the fact that predicted changes in the thermal component tend to reduce the convection strength in the LGM-5G simulation, this effect is overcompensated by the haline density contribution, in particular in the Labrador and Greenland Seas. This is clearly shown by the deepening of the convective layer depth and the density changes in the LGM-5G simulation (Figs. 5d,e). Furthermore, the LGM-5G NADW extends southward up to 30°S in a depth of about 5 km, which in turn avoids the intrusion of Antarctic Bottom Water (AABW) to the Northern Hemisphere. Nevertheless, the LGM-5G simulation delivers a weaker AABW formation rate as compared to the LGM-4G simulation. Due to small changes of oceanic surface conditions between the FLAT-5G and FLAT-4G simulations, the results of these experiments are not shown here. It must be noted, however, that the FLAT-5G simulation also predicts a slightly stronger NADW for-

mation rate compared to the FLAT-4G simulation. It is important to keep in mind that the LGM experiments discussed here do not take into account the background ablation from the ice sheets. This significant perturbation of the hydrological cycle may have severe consequences on the predicted strength of the thermohaline circulation (THC).

4. Summary and concluding remarks

This study provides a brief discussion of the atmospheric response to the new LGM paleotopography denoted ICE-5G (Peltier 2004). The comparison between the primary simulations performed with different ice sheet topographies shows that the new paleotopography, ICE-5G, generates an additional cooling over most of Canada and Eurasia compared to model predictions based upon the ICE-4G topography, whereas a warming is simulated over southern North America, the northwestern Atlantic, Greenland, northeastern Asia, and large parts of the SH ocean. The strong cooling over Canada is primarily a result of the lapse rate effect associated with the increased topographic height of the ICE-5G model compared to the ICE-4G precursor. It is important to note that snow–albedo feedback plays a secondary role despite the wintertime increase in snow accumulation in the LGM-5G simulation compared to LGM-4G. The topographic barrier imposed by the ICE-5G topography generates anomalous subtropical easterlies and produces a strengthened baroclinic zone over North America, as diagnosed from the Eady growth rate anomalies. This may play an important role in the storm-track activity as will be discussed in a forthcoming study in which a higher-resolution model of the atmospheric general circulation will be employed. Comparing the two simulations (LGM-5G and LGM-4G) with SST proxy data (Farrera et al. 1999) and lake-level reconstructions (Kohfeld and Harrison 2000) indicates some similarities.

The flat ice sheet simulations revealed that using the ICE-5G ice mask in place of the ICE-4G ice mask leads to warmer surface conditions as well as the generation of positive geopotential height anomalies over the NH polar region in the FLAT-5G compared to FLAT-4G simulation. In addition, the presence of lower albedo in eastern Eurasia strengthens the baroclinic activity and subsequently leads to wetter conditions as identified by enhanced precipitation in the FLAT-5G simulation. Climate changes related to changes of the ice sheet mask are considerably smaller as compared to the changes resulting from the topographic effect.

A number of the limitations of the modeling approach employed here originate from the assumptions on the basis of which the atmospheric model has been constructed, specifically the incorporation of only three atmospheric layers and the use of the quasigeostrophic approximation. However, Justino (2004) found that the presence of topography leads to an improved atmospheric circulation and stationary and transient wave activity with respect to a simulation that neglects orographic forcing. Some of the distinct observed features of stationary waves, that is, the Aleutian low, the low over Hudson Bay, and the high over the west coasts of North America and Europe, are well reproduced by ECBilt-Clio. It is also important to note, however, that compared to National Centers for Environmental Prediction (NCEP) reanalysis data the amplitude of the simulated stationary waves is reduced by a factor of 2. Moreover, the inclusion of the ice sheet topography in a three-layer atmosphere (200, 500, and 800 hPa) may be problematic. Compared with other coupled LGM simulations, however, the LGM-5G and LGM-4G experiments reveal large similarities with the results obtained from primitive equation multilayer models. To be more specific, the simulated stationary wave anomalies induced by LGM forcing are qualitatively and quantitatively very similar to those obtained by Kitoh et al. (2001) using the Meteorological Research Institute (MRI) CGCM. The same holds for the simulated SST structure. The upstream high and downstream low features associated with the presence of the ice sheets also show good agreement with, for example, Rind (1987; see his Fig. 22) and Broccoli and Manabe (1987; see their Fig. 11). The model is therefore able to reproduce the topographic responses much better than one might expect on a priori grounds.

Acknowledgments. A. Timmermann has been supported by the Japan Agency for Marine-Earth Science and Technology (JAMSTEC) through its sponsorship of the International Pacific Research Center. W. R. Peltier is supported by the Canadian Foundation for Climate and Atmospheric Science through the Polar Climate Stability Network and by the National Sciences and Engineering Research Council of Canada.

REFERENCES

Berger, A., 1978: A simple algorithm to compute long-term variations of daily and monthly insolation. Tech. Rep. 18, Institut d'Astronomique et de Géophysique, Université de Lauvain.

Broccoli, A., and S. Manabe, 1987: The influence of continental ice, atmospheric CO_2 and land albedo on the climate of the last glacial maximum. *Climate Dyn.,* **1,** 87–99.

Campin, J., and H. Goosse, 1999: A parameterization of dense overflow in large-scale ocean models in z coordinate. *Tellus,* **51A,** 412–430.

Cook, K., and I. Held, 1988: Stationary waves of the ice age climate. *J. Climate,* **1,** 807–819.

Crowley, T., 1995: Ice age terrestrial carbon changes revisited. *Global Biogeochem. Cycles,* **9,** 377–389.

Farrera, I., and Coauthors, 1999: Tropical climates at the last glacial maximum: A new synthesis of terrestrial palaeoclimate data. *Climate Dyn.,* **15,** 823–856.

Felzer, B., 2001: Climate impacts of an ice sheet in East Siberia during the Last Glacial Maximum. *Quat. Sci. Rev.,* **20,** 437–447.

Gent, P., and J. McWilliams, 1990: Isopycnal mixing in ocean general circulation models. *J. Phys. Oceanogr.,* **20,** 150–155.

Goosse, H., and T. Fichefet, 1999: Importance of ice-ocean interactions for the global ocean circulation: A model study. *J. Geophys. Res.,* **104** (C10), 23 337–23 355.

——, E. Deleersnijder, T. Fichefet, and M. England, 1999: Sensitivity of a global coupled ocean-sea ice model to the parameterization of vertical mixing. *J. Geophys. Res.,* **104** (C6), 13 681–13 695.

——, F. Selten, R. Haarsma, and J. Opsteegh, 2003: Large sea-ice volume anomalies simulated in a coupled climate model. *Climate Dyn.,* **10,** doi:10.1007/s00382-002-0290-4.

Held, I., and M. Suarez, 1978: A two-level primitive equation atmosphere model designed for climate sensitivity experiments. *J. Atmos. Sci.,* **35,** 206–229.

Hewitt, C. D., A. Broccoli, J. Mitchell, and R. J. Stouffer, 2001: A coupled model of the last glacial maximum: Was part of the North Atlantic relatively warm? *Geophys. Res. Lett.,* **28,** 1571–1574.

Holton, J. R., 1993: *Introduction to Dynamic Meteorology.* Academic Press, 511 pp.

Justino, F., 2004: *The Influence of Boundary Conditions on the Last Glacial Maximum.* Shaker Verlag, 127 pp.

——, A. Timmermann, U. Merkel, and E. Souza, 2005: Synoptic reorganization of atmospheric flow during the Last Glacial Maximum. *J. Climate,* **18,** 2826–2846.

Kageyama, M., and P. Valdes, 2000: Impact of the North American ice-sheet orography on the last glacial maximum eddies and snowfall. *Geophys. Res. Lett.,* **27,** 1515–1518.

Kasahara, A., T. Sasamori, and W. Washington, 1973: Simulation experiments with a 12-layer stratospheric global circulation model. I. Dynamical effect of the Earth's orography and thermal influence of continentality. *J. Atmos. Sci.,* **30,** 1229–1251.

Kitoh, A., 1997: Mountain uplift and surface temperature changes. *Geophys. Res. Lett.,* **24,** 185–188.

——, 2004: Effects of mountain uplift on East Asia summer climate investigated by a coupled atmosphere–ocean GCM. *J. Climate,* **17,** 783–802.

——, S. Mukarami, and H. Koide, 2001: A simulation of the Last Glacial Maximum with a coupled atmosphere-ocean GCM. *Geophys. Res. Lett.,* **28,** 2221–2224.

Kohfeld, K., and S. Harrison, 2000: How well can we simulate past climates? Evaluating the models using palaeoenvironmental datasets. *Quat. Sci. Rev.,* **19,** 321–346.

Kutzbach, J., and P. Guetter, 1986: The influence of changing orbital parameters and surface boundary conditions on climate simulations for the past 18 000 years. *J. Atmos. Sci.,* **43,** 1726–1759.

Lindzen, R., and B. Farrell, 1980: A simple approximate result for maximum growth rate of baroclinic instabilities. *J. Atmos. Sci.,* **37,** 1648–1654.

Manabe, S., and T. Terpstra, 1974: The effects of mountains on the general circulation of the atmosphere as identified by numerical experiments. *J. Atmos. Sci.,* **31,** 3–42.

——, and A. Broccoli, 1985: The influence of continental ice sheets on the climate of an ice age. *J. Geophys. Res.,* **90,** 2167–2190.

Marshall, J., and F. Molteni, 1993: Toward a dynamic understanding of planetary-scale flow regimes. *J. Atmos. Sci.,* **50,** 1792–1818.

McManus, J., R. Francois, J.-M. Gherardi, L. Keigwin, and S. Brown-Leger, 2004: Collapse and rapid resumption of Atlantic meridional circulation linked to deglacial climate changes. *Nature,* **428,** 834–837.

Mellor, G., and T. Yamada, 1982: Development of a turbulence closure model for geophysical fluid problems. *Rev. Geophys. Space Phys.,* **20,** 851–875.

Opsteegh, J., R. Haarsma, F. Selten, and A. Kattenberg, 1998: ECBILT: A dynamic alternative to mixed boundary conditions in ocean models. *Tellus,* **50A,** 348–367.

Peltier, W., 1994: Ice age paleotopography. *Science,* **265,** 195–201.

——, 2004: Global glacial isostasy and the surface of the ice-age Earth: The ICE-5G (VM2) model and GRACE. *Annu. Rev. Earth Planet. Sci.,* **32,** 111–149.

——, and L. Solheim, 2004: The climate of the Earth at Last Glacial Maximum: Statistical equilibrium state and a mode of internal variability. *Quat. Sci. Rev.,* **23,** 335–357.

——, I. Shennan, R. Drummond, and B. Horton, 2002: On the postglacial isostatic adjustment of the British Isles and the shallow viscoelastic structure of the Earth. *Geophys. J. Int.,* **148,** 443–475.

Rind, D., 1987: Components of the ice age circulation. *J. Geophys. Res.,* **92,** 4241–4281.

Schäfer-Neth, C., and A. Paul, 2003: The Atlantic Ocean at the Last Glacial Maximum: 1. Objective mapping of the GLAMAP sea-surface conditions. *Paleoceanography,* **18,** 1058, doi:10.1029/2002PA000783.

Schmitt, R., P. Bogden, and C. Dorman, 1989: Evaporation minus precipitation and density flux for the North Atlantic. *J. Phys. Oceanogr.,* **19,** 1208–1221.

Seager, R., D. Battisti, J. Yin, N. Gordon, N. Naik, C. Clement, and M. Cane, 2002: Is the Gulf Stream responsible for Europe's mild winters? *Quart. J. Roy. Meteor. Soc.,* **128,** 2563–2586.

Speer, K., and E. Tziperman, 1992: Rates of water mass formation in the North Atlantic Ocean. *J. Phys. Oceanogr.,* **22,** 94–104.

Tarasov, L., and W. Peltier, 2002: Greenland glacial history and local geodynamic consequences. *Geophys. J. Int.,* **150,** 198–229.

Timmermann, A., F. Justino, F.-F. Jin, and H. Goosse, 2004: Surface temperature control in the North and tropical Pacific during the last glacial maximum. *Climate Dyn.,* **23,** 353–370.

Vettoretti, G., W. R. Peltier, and N. A. McFarlane, 2000: Global water balance and atmospheric water vapour transport at Last Glacial Maximum: Climate simulations with the CCCma atmospheric general circulation model. *Can. J. Earth Sci.,* **37,** 695–723.

Veum, T., E. Jansen, M. Arnold, I. Beyer, and J. Duplessy, 1992: Water mass exchange between the North Atlantic and the Norwegian Sea during the past 28 000 years. *Nature,* **356,** 783–785.